SMALL-SCALE ASSESSMENT OF CORROSION-INDUCED DAMAGE IN HARDMETALS

Y. F. Zheng[1,2,*,Φ], G. Fargas[1,2], H. Besharatloo[1,2], J. J. Roa[1,2], O. Lavigne[3], L. Llanes[1,2]

[1]CIEFMA, Departament de Ciència dels Materials i Enginyeria Metal·lúrgica, Universitat Politècnica de Catalunya, EEBE, Barcelona 08019, Spain
[2] Barcelona Research Center in Multiscale Science and Engineering, Universitat Politècnica de Catalunya, Barcelona 08019, Spain
[3] Hyperion Materials & Technologies, 08107 Martorelles, Spain

* Corresponding author, e-mail: yafeng.zheng@upc.edu
Φ Current address: Escola d'Enginyeria de Barcelona Est (EEBE), Campus Diagonal Besòs, Edifici I, Av. Eduard Maristany 16, 08019 Barcelona

Abstract

In this work, the effect of corrosion-induced damage on mechanical response of hardmetals was evaluated at small-scale level by nanoindentation and nanoscratch techniques. Immersion tests in acidic solution were performed to induce corrosion damage in a controlled way. Results pointed out that the corroded zone led to a strong reduction of hardness and elastic modulus compared to the non-corroded samples. Significant differences were also observed in nanoscratch tracks not only regarding width and depth but also deformation mechanisms developed, as scratching load increased. Corroded surfaces displayed relevant damage even a quite low loads (~45 mN). Cracking and fragmentation of individual WC grains took place together with chipping of fine WC fragments at the track edges. Such microstructural degradation was detected for non-corroded specimens at much higher loads (~400 mN).

Keywords: Hardmetals, corrosion, nanoindentation, nanoscratch.

1. Introduction

Cemented carbides, also simply referred to as hardmetals, has been extensively used as a tooling material in manufacturing and mining industries due to their outstanding combination of hardness, wear resistance and toughness [1-3]. They are composite materials comprising hard ceramic phase (generally WC) in a more ductile metallic binder. In general, the preferential choice for the ductile binder is Co. However, it is also common to choose binders of different chemical nature (e.g. Ni, CoNi) for applications demanding enhanced performance when subjected to severe working conditions, such as corrosive environment and high temperature [4]. Additionally, the mechanical and in-service performance can be tuned by adjusting the carbide grain size, binder content and composition [1,4,5].

As a rule, poor corrosion resistance of cemented carbides is a key factor limiting its application in chemically aggressive environments [6-8]. For this reason, the corrosion behaviour of hardmetals has been intensively investigated in recent decades [5-11]. It has been demonstrated that corrosive media preferentially attacks the binder phase when exposed to acidic and neutral environments, due to the galvanic coupling between the carbides and binder phase [9-12]. In alkaline solution, Co binder exhibits stable passivation, while WC phase is readily dissolved [5, 10-12]. Normally, corrosion damage induced by acidic media is much more severe than that from neutral and basic ones, which can be reflected in much higher current density [10] and wear rate [11,12]. A greater amount of binder phase dissolution in acidic solution ultimately results in the formation of W oxide layer and Co-depleted region, compared to exposure in neutral and basic solutions [9]. The formed corroded layer is no longer present in the compact form as shown in the uncorroded hardmetals, which leads to a pronounced deterioration in the mechanical and in-service performance of cemented carbides. In this regard, numerous investigations have been done for determining the detrimental effects of aggressive acidic environment on flexural strength [6], wear resistance [8, 11, 12] and fatigue resistance [13]. However, scarce information can be found regarding microstructural degradation phenomena occurring on the surface and its influence on mechanical response of cemented carbides. In recent years, nanoindentation and nanoscratch techniques have drawn much attention and have been extensively used to comprehend the mechanical behavior of materials at micron- and submicron length scale. Concerning this study, implementation of nanoindentation technique has mainly focused on the measurements of Young's modulus (E) and hardness (H) in constituent phases of hardmetals, as well as on the evaluation of crystal orientation effects for WC single

crystals [14-19]. On the other hand, nanoscratch testing has proven to be useful for understanding tribomechanical response (e.g. deformation, wear and removal mechanism) of cemented carbides [20-22].

Following the above ideas, in this work the influence of corrosion-induced damage on the small-scale mechanical properties of the studied hardmetal was assessed by means of nanoindentation and nanoscratch tests. In doing so, controlled corrosion damage was induced by immersing the material in stirred acidic solution. Special emphasis was placed on documenting deformation and damagel mechanisms of the non-corroded and corroded surfaces. Finally, residual imprints and scratch tracks were deeply analyzed by focused ion beam/field emission scanning electron microscopy (FIB/FESEM).

2. Experimental procedure

One medium grain sized hardmetal grade supplied by Hyperion Materials and Technologies company was tested in this study. Key microstructural parameters including binder content ($\%_{wt.}$), mean grain size (d_{WC}), contiguity (C_{WC}) and binder mean free path (λ_{binder}) are detailed in **Table 1**. Mean grain size was measured by the linear intercept method, using FESEM micrographs. Carbide contiguity and binder mean free path were deduced following empirical relationship given in the literature [23].

Table 1. *Microstructural parameters for the investigated cemented carbide.*

wt.% Co	d_{WC} (μm)	C_{WC}	λ_{binder} (μm)
6	1.51±0.16	0.48±0.02	0.32±0.03

Controlled corrosion-induced damage was performed by immersion test in stirred 0.1M HCl solution at room temperature. A long exposure time (264 h) was selected in order to obtain a pronouncedly degraded microstructure. Before and after immersion tests, the specimens were hand-cleaned using soapy water, then ultrasonically cleaned for 15 min in ethanol, and subsequently dried in the air, finally used for the nanoindentation and nanoscratch tests.

Nanoindentation tests were performed on uncorroded and corroded surfaces using Berkovich diamond indenter at a constant strain rate 0.05 s^{-1}, and indentations were made to a maximum load of 650 mN. The measurements were repeated 25 times for obtaining a more reliable average. Moreover, nanoscratch tests were conducted on the same samples under two different conditions. One corresponded to a maximum load of 60 mN and scratch length of 60 μm (corresponding to a loading rate of 1 mN/s). The other involved a maximum load of 500 mN and scratch length of 200 μm (corresponding to a loading rate of 2.5 mN/s). In addition, the residual imprints and scratch tracks were further observed and analyzed by mean of FIB/FESEM.

3. Results and discussion

3.1. Nanoindentation

The typical load-displacement curves recorded from Berkovich indentation with the maximum load of 650 mN are given in **Figure 1**. Corrosion-induced damage has a significant effect on *P-h* behavior of studied grade, which is reflected in the obvious increase of the maximum penetration depth from 1196 nm to 1496 nm. In addition, the indentation damage displays in different forms, as shown in **Figure 2**. For the non-corroded surface, deformed WC grains, as well as few microfractures, are discerned (**Figure 2a**). However, in the case of corroded surface, in addition to the deformed grains, the damage is mainly manifested in the form of grain pull-out and breakaway of unsupported grains (**Figure 2b**). The mechanical support for the WC in the surface layer is reduced due to the dissolution of Co binder. The remained WC skeleton can no longer withstand a mechanical force like the compact non-corroded surface, and these loose grains can be easily removed.

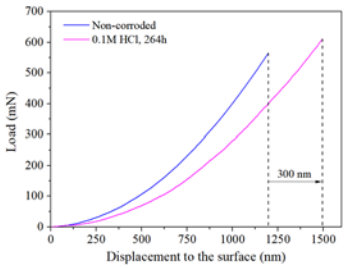

Figure 1. Representative indentation load-displacement curves from Berkovich indentation.

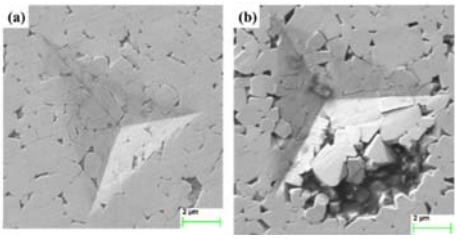

Figure 2. Residual imprints made on the (a) non-corroded and (b) corroded surfaces.

Figure 3 shows Young's modulus and hardness as a function of penetration depth measured from non-corroded and corroded surfaces. It is clearly seen that the values are stabilised from penetration depth larger than 500 nm. Before this point, the mesured values display considerable scatter due to the surface defects and roughness. Mechanical properties of the studied grade are pronouncedly degraded due to corrosion-induced damage caused by exposure in 0.1M HCl solution. With respect to the non-corroded sample, Young's modulus of 679 GPa and a hardness of 24 GPa were obtained. In contrast, the corroded sample displayed much lower values, 464 GPa and 15 GPa respectively.

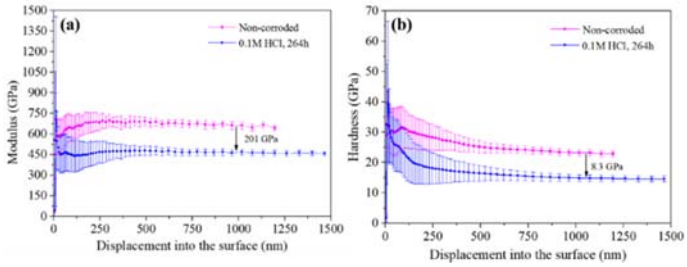

Figure 3. Young's modulus (a) and hardness (b) as a function of penetration depth for non-corroded and corroded samples.

Figure 4 shows FIB cross-sectional scenarios of the nanoindentation imprints made on the non-corroded and corroded surfaces. For the non-corroded material, the existing Co phase absorbs the energy from indented damage, and then protects the carbides from cracking. When subjected to impacting conditions, the enhanced fracture toughness of cemented carbides, which is generally attributed to the deformation of metallic binder phase, is highly demanded. The deformation of binder phase is usually achieved by mechanical twinning, planar slip and/or phase transformation [24-27]. During the deformation process, the binder with fcc modification deforms through the formation of hcp lamellae, which is related to the glide of partial dislocations [28]. When the deformation proceeds to a certain extent, the movement of dislocation is hindered due to the work hardening, which leads to a decrease in the capability of preventing crack propagation hence the compatibility of plastic accommodation [28]. Simultaneously a glide mechanism also occurs in each of the plastically deformed WC grains, eventually leading to grain breakage and cracking (see **Figure 4a**). This is in agreement with the previous studies [28]. Regarding the corroded sample, a deformed carbides skeleton with cracks in carbides surrounding the imprints is discerned (**Figure 4b**). In this case, FIB/FESEM cross-sectional micrograph reveals a WC skeleton under the analysed imprint with no presence of binder for the first 16 µm. This significantly changes its deformation behavior compared to the non-corroded material (**Figure 4a**). Without the protection from the ductile phase, the indentation damage appears to first cause the pore filling, and then the indentation stress accumulates directly on the WC grain surrounding the imprint, ultimately resulting in a more severe microfracture scenario.

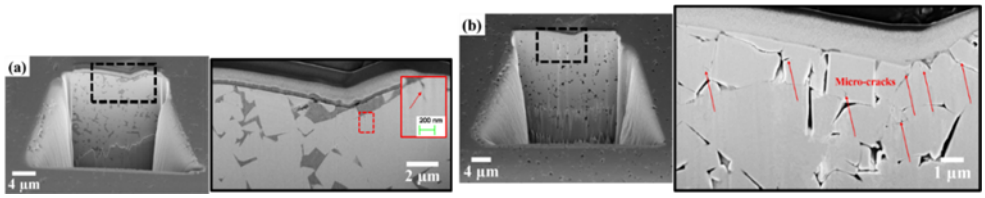

Figure 4. FIB cross-sectional images of the residual imprints made on (a) non-corroded and (b) corroded surfaces.

3.2. Nanoscratch

Figure 5 reveals different scratched scenarios associated with the non-corroded and corroded textures, in which the related failure events (e.g. spallation, cracking) can be clearly discerned. The non-corroded texture displays a much better scratch tolerance, in view of the scratch width and the spallation degree. In this case,

a clear groove is discerned, and the edges of the groove have piled up with debris and some crushed particles. This is attributed to the binder squeeze-out and the WC grain pull-out induced during the scratch test [22]. In the latter case, a rougher morphology, as well as a larger lump piling up near the groove edge, is discerned. The observed fragmentation of fine WC fragments at the edge of the track appears to be accompanied by the entire scratch. In addition, a larger scratch width is discerned as the increased scratching load.

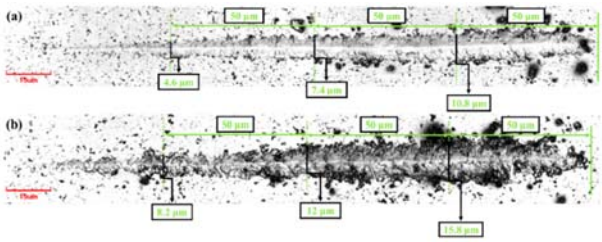

Figure 5. LSCM micrographs of two scratch tracks performed on (a) non-corroded sample and (b) corroded sample after being immersed in 0.1M HCl solution for 264h.

The corresponding scratch load-penetration depth curves resulting from nanoscratch testing are presented in **Figure 6**. As the load increases, both samples exhibit a raising penetration depth. Once corroded, the scratching penetration for a given applied load is significantly increased. This is consistent with the increased penetration depth illustrated in the nanoindentation test. Under given nanoscratch condition, deeper penetration inevitably results in the larger damaged area (**Figure 5b**).

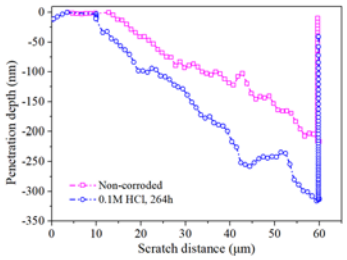

Figure 6. Curves of indenter penetration depth as a function of scratch distance.

In order to have a clear picture of the deformation and removal mechanism, a further analysing along the scratch track was carried out by means of FESEM technique. **Figure 7** gives the first observed microfracture from two studied scratch tracks. For the non-corroded surface, the obvious microfracture originates from the load of ~60 mN, at which load range no significant grain pull-out can be discerned (**Figure 7a**). In contrast, the scratch on the corroded surface displays a more severe damaged scenario, where cracking and fragmentation of individual WC grains occurred with chipping of fine WC fragments at the track edges are discerned at a lower scratch load (~45 mN), as illustrated in **Figure 7b**. In the former case, the presence of Co phase consumes the energy from scratching through its own deformation [22]. This delays the generation of the microfracture and grain pull-out. However, in the latter case, the increasing strain caused by scratching appears to accumulate directly on individual WC grains, making them more susceptible to cracking, chipping and eventually pull-off.

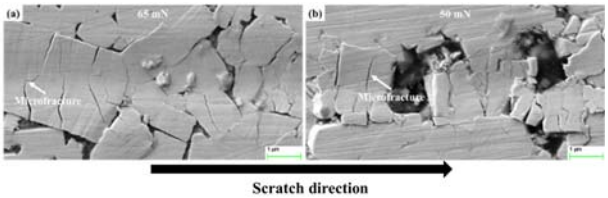

Figure 7. FESEM images showing first observation of microfracture along the scratch track in (a) the non-corroded sample and (b) corroded sample after being immersed in 0.1M HCl solution for 264h

Damage appearance and evolution are shown in **Figure 8** for three load levels: 125 mN, 250 mN and 375 mN. It is evident that there are considerable differences in the response of the scratch damage depending on the presence of Co binder or not. For the texture containing Co phase, the strain induced by scratching is initially released by the plastic deformation and removal of the ductile binder phase (via squeeze-out) from the surface layer. Meanwhile, the strain gradually accumulates on the WC grains as the scratch load increases. When the accumulated strain reached a critical value, the microfracture generated in the WC grains (**Figure 7a**). Subsequently, the damaged scenarios are dominated by the fragmentation of individual WC grains,

accompanied by the re-embedding of WC fragments into the deformed Co phase (**Figure 8a**). This damage mechanism is in agreement with previous studies [21, 22, 29-31]. After being corroded, there are only WC skeletons left, thereby the plastic strain accumulates directly on the WC grains from the initial stage of the scratch test, making them more susceptible to breakage even under relatively small load conditions. Subsequently, a series of further damage occurs as the scratch load increases, such as grain chipping, delaminating and pull-off (**Figure 8b**).

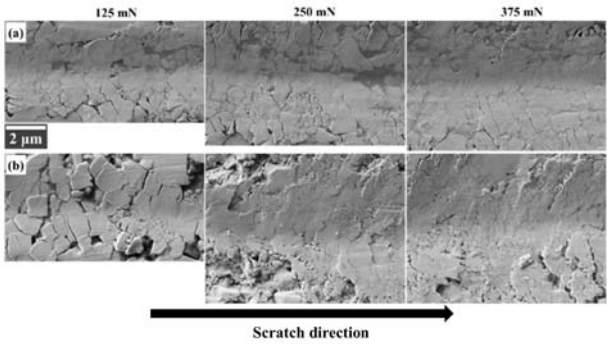

Figure 8. Scratch track view associated with three different applied load levels: 125 mN, 250 mN and 375 mN, for (a) non-corroded and (b) corroded surfaces.

4. Conclusions

In this study, the corrosion damage induced by immersion test in acidic solution was assessed on the basis of the mechanical response at micrometric length scale by means of nanoindentation and nanoscratch tests. Main conclusions drawn may be summarized as follows:

- It was demonstrated that nanoindentation measurements allow evaluating the effect of corrosion-induced damage on mechanical properties. Hardness and Young's modulus was strongly reduced down to 37% and 32% respectively in acidic solution. FIB observation corresponding to the corroded surface reveals a deformed carbides skeleton with cracks in carbides surrounding the imprints.

- The sliding contact responses of non-corroded and corroded surfaces are found to exhibit a significant difference in the nanoscratch tracks not only regarding width and depth but also deformation mechanisms developed as increasing progressively the scratching load. In the former case, a more plastically deformed track morphology is discerned due to the existing Co phase. In the latter case, cracking and fragmentation of WC grains start from a lower load level (~45 mN) and appear to run through the entire scratch track.

ACKNOWLEDGEMENTS

This work was financially supported by the collaborative Industry-University program between Hyperion Materials & Technologies and Universitat Politècnica de Catalunya, and partly funded by the Spanish Ministerio de Economía y Competividad through Grant MAT2015-70780-C4-3-P (MINECO/FEDER). Additionally, Y. F. Zheng acknowledges the Ph.D. scholarship received from China Scholarship Council.

References

[1] H. E. Exner, Physical and chemical nature of cemented carbides, Int. Met. Rev. 24 (1979) 149-173.
[2] B. Roebuck, E.A. Almond, Deformation and fracture processes and the physical metallurgy of WC-Co hardmetals, Int. Mater. Rev. 33 (1988) 90-110.
[3] G. S. Upadhyaya, Materials science of cemented carbides-an overview, Mater. Des. 22 (2001) 483-489.
[4] V. A. Tracey, Nickel in hardmetals, Int. J. Refract. Met. Hard Mater. 11(1992) 137-149.
[5] F. J. J. Kellner, H. Hildebrand, S. Virtanen, Effect of WC grain size on the corrosion behaviour of WC-Co based hardmetals in alkaline solutions, Int. J. Refract. Met. Hard Mater. 27 (2009) 806-812.
[6] V. A. Pugsley, G. Korn, S. Luyckx, H. G. Sockel, W. Heinrich, M. Wolf, H. Feld, R. Schulte, The influence of a corrosive wood-cutting environment on the mechanical properties of hardmetal tools, Int. J. Refract. Met. Hard Mater. 19 (2001) 311-318.
[7] M. Bjordal, E. Bardal, T. Rogne, T. G. Eggen, Erosion and corrosion properties of WC coatings and duplex stainless steel in sand-containing synthetic sea water, Wear 186-187 (1995) 508-514.

[8] S. Sutthiruangwong, G. Mori, R. Kösters, Passivity and pseudopassivity of cemented carbides, Int. J. Refract. Met. Hard Mater. 23 (2005) 129-136.
[9] S. Sutthiruangwong, G. Mori, Corrosion properties of Co-based cemented carbides in acidic solutions. Int. J. Refract. Met. Hard Mater. 21(2003) 135-145.
[10] S. Hochstrasser(-Kurz), Y. Mueller, C. Latkoczy, S. Virtanen, P. Schmutz, Analytical characterization of the corrosion mechanisms of WC-Co by electrochemical methods and inductively coupled plasma mass spectroscopy, Corros. Sci. 49 (2007) 2002-2020.
[11] H. Engqvist, U. Beste, N. Axén, The influence of pH on sliding wear of WC-based materials, Int. J. Refract. Met. Hard Mater. 18 (2000) 103-109.
[12] A. J. Gant, M. G. Gee, A.T. May, The evaluation of tribo-corrosion synergy for WC-Co hardmetals in low stress abrasion, Wear 256 (2004) 500-516.
[13] V. A. Pugsley, H. G. Sockel, Corrosion fatigue of cemented carbide cutting tool materials, Mater. Sci. Eng. A 366 (2004) 87-95.
[14] M. Gee, B. Roebuck, P. Lindahl, H. Andren, Constituent phase nanoindentation of WC/Co and Ti (C, N) hard metals, Mater. Sci. Eng. A 209 (1996) 128-136.
[15] A. Duszová, R. Halgaš, M. Bľanda, P. Hvizdoš, F. Lofaj, J. Dusza, J. Morgiel, Nanoindentation of WC-Co hardmetals, J. Eur. Ceram. Soc. 33 (2013) 2227-2232.
[16] J. J. Roa, E. Jiménez-Piqué, J. M. Tarragó, M. Zivcec, C. Broeckmann, L. Llanes, Berkovich nanoindentation and deformation mechanisms in a hardmetal binder-like cobalt alloy, Mater. Sci. Eng., A 621 (2015) 128-132.
[17] J. J. Roa, E. Jimenez-Pique, C. Verge, J. M. Tarragó, A. Mateo, J. Fair, L. Llanes, Intrinsic hardness of constitutive phases in WC-Co composites: Nanoindentation testing, statistical analysis, WC crystal orientation effects and flow stress for the constrained metallic binder, J. Eur. Ceram. Soc. 35 (2015) 3419-3425.
[18] C. A. Botero, E. Jimenez-Piqué, R. Martín, T. Kulkarni, V. K. Sarin, L. Llanes, Nanoindentation and nanoscratch properties of mullite-based environmental barrier coatings: Influence of chemical composition-Al/Si ratio, Surf. Coat. Tech. 239 (2014) 49-57.
[19] A. Dey, R. Umarani, H. Thota, P. Bandyopadhyay, A. Rajendra, A. Sharma, A. K. Mukhopadhyay, Corrosion and nanoindentation studies of MAO coatings, Surf. Eng. 30 (2014) 913-919.
[20] R. Irwan, H. Huang, Removal and fracture characteristics of cemented tungsten carbide under nanoindenting and nanoscratching, Adv. Mater. Res. 447-448 (2009) 16-20.
[21] S. Ndlovu, K. Durst, M. Göken, Investigation of the sliding contact properties of WC-Co hard metals using nanoscratch testing, Wear 263 (2007) 1602-1609.
[22] H. Q. Sun, R. Irwan, H. Huang, G. W. Stachowiak, Surface characteristics and removal mechanism of cemented tungsten carbides in nanoscratching, Wear 268 (2010) 1400-1408.
[23] J. M. Tarragó, D. Coureaux, Y. Torres, F. Yu, I. Al-Dawery, L. Llanes, Implementation of an effective time-saving two-stage methodology for microstructural characterization of cemented carbides, Int. J. Refract. Met. Hard Mater. 55 (2016) 80-86.
[24] B. Roebuck, E. A. Almond, The influence of composition, phase transformation and varying the relative F.C.C. and H.C.P. phase contents on the properties of dilute Co-W-C Alloys, Mater. Sci. Eng. A 66 (1984) 179-194.
[25] C. H. Vasel, A. D. Krawitz, E. F. Drake, E. A. Kenik, Binder deformation in WC-(Co,Ni) cemented carbide composites, Metall. Mater. Trans. A 16 (1985) 2309-2317.
[26] G. Erling, S. Kursawe, S. Luyck, H. G. Sockel, Stable and unstable fracture surface features in WC-Co, J. Mater. Sci. Lett. 19 (2000) 437-438.
[27] T. Takahashi, E. J. Friese, Determination of the slip systems in single crystals of tungsten monocarbide, Philos. Mag. 12 (1965) 1-8.
[28] V. K. Sarin, T. Johannesson, On the deformation of WC-Co cemented carbides, Meter. Sci. 9 (1975) 472-476.
[29] J. Heinrichs, M. Olsson, S. Jacobson, Surface degradation of cemented carbides in scratching contact with granite and diamond-the roles of microstructure and composition, Wear 342 (2015) 210-221.
[30] M. Gee, K. Mingard, J. Nunn, B. Roebuck, A. Gant, In situ scratch testing and abrasion simulation of WC/Co. Int. J. Refract. Met. Hard Mater. 62 (2017) 192-201.
[31] M. Gee, A. Gant, B. Roebuck, Wear mechanisms in abrasion and erosion of WC/Co and related hardmetals, Wear 263 (2007) 137-148.